Monthly Notices of the ROYAL ASTRONOMICAL SOCIETY

MNRAS **548,** 1–9 (2026)
Advance Access publication 2026 February 3

https://doi.org/10.1093/mnras/stag224

Detection of an extremely luminous radio counterpart to the Be/X-ray binary A0538−66

Justine Crook-Mansour [1]★, Rob Fender,[1,2] Alex Andersson [1], Hao Qiu [3], Andrew K. Hughes [1], Jakob van den Eijnden [4], Fraser J. Cowie [1], Sara Motta,[1,5] Itumeleng Monageng [2,6], Lorenzo Ducci [7], Sandro Mereghetti [8], Andries Mathiba,[2,6] Dougal Dobie [9,10], Tara Murphy [9,10], David L. Kaplan [11], Francesco Carotenuto [12] and Phil Charles[1,13,14]

[1]*Astrophysics, Department of Physics, University of Oxford, Keble Road, Oxford OX1 3RH, UK*
[2]*Department of Astronomy, University of Cape Town, Private Bag X3, Rondebosch 7701, South Africa*
[3]*SKA Observatory, Jodrell Bank, Lower Withington, Macclesfield SK11 9FT, UK*
[4]*Anton Pannekoek Institute for Astronomy, Universiteit van Amsterdam, Science Park 904, NL-1098 XH Amsterdam, the Netherlands*
[5]*Istituto Nazionale di Astrofisica (INAF), Osservatorio Astronomico di Brera, Via E. Bianchi 46, I-23807 Merate (LC), Italy*
[6]*South African Astronomical Observatory, PO Box 9, Observatory, Cape Town 7935, South Africa*
[7]*Institut für Astronomie und Astrophysik, Kepler Center for Astro and Particle Physics, Universität Tübingen, Sand 1, D-72076 Tübingen, Germany*
[8]*INAF – Istituto di Astrofisica Spaziale e Fisica Cosmica, Via A. Corti 12, I-20133 Milano, Italy*
[9]*Sydney Institute for Astronomy, School of Physics, The University of Sydney, Sydney, NSW 2006, Australia*
[10]*ARC Centre of Excellence for Gravitational Wave Discovery (OzGrav), Hawthorn, VIC 3122, Australia*
[11]*Center for Gravitation, Cosmology, and Astrophysics, Department of Physics & Astronomy, University of Wisconsin-Milwaukee, PO Box 413, Milwaukee, WI 53201, USA*
[12]*INAF, Osservatorio Astronomico di Roma, Via Frascati 33, I-00078 Monte Porzio Catone, Italy*
[13]*Department of Physics & Astronomy, University of Southampton, Southampton SO17 1BJ, UK*
[14]*Department of Physics, University of the Free State, PO Box 339, Bloemfontein 9300, South Africa*

Accepted 2026 January 26. Received 2026 January 19; in original form 2025 November 21

ABSTRACT

We present the discovery of radio emission from the Be/X-ray binary A0538−66 with the Australian Square Kilometre Array Pathfinder, and results from a subsequent weekly monitoring campaign with the MeerKAT radio telescope. A0538−66, located in the Large Magellanic Cloud, hosts a neutron star with a short spin period ($P \approx 69$ ms) in a highly eccentric ≈ 16.6-d orbit . Its rare episodes of super-Eddington accretion, rapid optical and X-ray flares, and other peculiar properties make it an interesting system among high-mass X-ray binaries. Our MeerKAT data reveal that it is also one of the most radio-luminous neutron star X-ray binaries observed to date, reaching $\approx 3 \times 10^{22}$ erg s^{-1} Hz^{-1} (at 1.28 GHz), with radio emission that appears to be orbitally modulated. We consider several possible mechanisms for the radio emission, and place A0538−66 in context by comparing it to similar systems.

Key words: accretion, accretion discs – stars: neutron – X-rays: binaries – X-rays: individual: A0538−66.

1 INTRODUCTION

X-ray binaries (XRBs) are bright X-ray sources in which a compact object – either a neutron star (NS) or black hole (BH) – accretes matter from a stellar binary companion (donor star). *Be/X-ray binaries* (Be/XRBs; see P. Reig 2011 for a review) are a type of high-mass X-ray binary (HMXB) hosting an NS accreting material from an early-type Oe/Be star of luminosity class III–V. The emission lines in the donor star's optical spectra (most commonly studied are the Balmer and Paschen series) and enhanced infrared radiation indicate the presence of a disc of dense gas lying in the equatorial plane of the donor star, known as the *circumstellar/decretion disc*. Accretion-driven outbursts are classically divided into two types: *Type I* outbursts,[1] occur when the NS intersects the Be star's decretion disc near periastron, leading to episodic accretion and typical peaks of $L_X \lesssim 10^{37}$ erg s^{-1} (e.g. A. T. Okazaki & I. Negueruela 2001), while *Type II* (giant) outbursts may last multiple orbital cycles and can reach (super-)Eddington luminosities (e.g. Y. Moritani et al. 2013).

A0538−66 (also known as 1A 0535−668) is a Be/XRB in the Large Magellanic Cloud (LMC; $D \approx 50$ kpc; G. Pietrzyński et al. 2019) that was discovered in 1977 when the *Ariel V* satellite detected two X-ray outbursts separated by ∼17 d (N. E. White & G. F.

★ E-mail: justine.crook-mansour@physics.ox.ac.uk

[1]Not to be confused with 'Type I X-ray bursts' in low-mass X-ray binaries (LMXBs).

Carpenter 1978). The system contains an NS in a highly eccentric orbit ($e \approx 0.72$), with a period of $P_{\rm orb} \approx 16.6$ d around a B1 IIIe donor (A. F. Rajoelimanana et al. 2017). The inclination of the binary plane to our line of sight is constrained to be high (but $\lesssim 75^\circ$, owing to the absence of X-ray eclipses), while the decretion disc is inferred to be misaligned with respect to this and may precess (A. F. Rajoelimanana et al. 2017; R. G. Martin & P. A. Charles 2024).

The source undergoes X-ray outbursts occurring on a range of time-scales, with luminosities spanning five orders of magnitude in dynamical range. In the years following its discovery, several X-ray events were reported to exceed the isotropic Eddington limit (for an NS, $L_{\rm Edd} \sim 10^{38}$ erg s^{-1}; e.g. N. E. White & G. F. Carpenter 1978), whereas later observations found lower luminosities ($\sim 10^{33\text{-}37}$ erg s^{-1}; e.g. S. Campana et al. 2002, P. Kretschmar et al. 2004).[2] However, in 2018, the source once again reached Eddington levels (with a peak 0.2–10 keV luminosity of $\sim 4 \times 10^{38}$ erg s^{-1}; L. Ducci, S. Mereghetti & A. Santangelo 2019b). During this time, it exhibited rapid, strong X-ray flares near periastron – with flux changes of up to three orders of magnitude on time-scales of a few seconds – which may be attributed to very fast switches between spherical accretion and supersonic propeller regimes (L. Ducci et al. 2019b; M. Rigoselli et al. 2025). Occasionally, the source exhibits X-ray flares far from periastron, which could be due to a warped decretion disc (supported by observations from A. F. Rajoelimanana et al. 2017) or inhomogeneities/clumps in the surrounding circumstellar environment (L. Ducci et al. 2022). On 2025 September 30, the source again reached super-Eddington levels, with a 0.2–12 keV luminosity of $\sim 1.5 \times 10^{39}$ erg s^{-1} (L. Ducci, S. Mereghetti & M. Bachetti 2025).

A0538−66 displays X-ray pulsations at ∼69 ms (G. K. Skinner et al. 1982; L. Ducci & S. Mereghetti 2025), making it the fastest spinning accretion-powered NS in a HMXB.[3] Interestingly, these pulsations have only been detected three times: during a super-Eddington outburst in 1980 (G. K. Skinner et al. 1982), in a single ∼11-min observation in January 2023 at a much lower luminosity ($L_{\rm X} \sim 8 \times 10^{36}$ erg s^{-1}, 0.3–10 keV; L. Ducci & S. Mereghetti 2025), and during the super-Eddington outburst in September 2025 (L. Ducci et al. 2025). Their sporadic appearance has been attributed to plasma temporarily leaking through the centrifugal barrier via an instability mechanism, allowing accretion onto the polar caps (L. Ducci & S. Mereghetti 2025).

The source's optical outbursts also vary widely in amplitude and duration, reaching some of the brightest levels seen in HMXBs ($L_{\rm opt} \sim 3 \times 10^{38}$ erg s^{-1}; G. K. Skinner 1980), likely primarily powered by the reprocessing of X-rays in an envelope of dense gas surrounding the donor star (L. Ducci et al. 2019a). Its optical emission is orbitally modulated (G. K. Skinner 1980), with double-peaked profiles near periastron supporting a disc–plane misalignment (e.g. A. F. Rajoelimanana et al. 2017; L. Ducci & S. Mereghetti 2025). The source also displays irregular optical variability on ∼day time-scales, possibly caused by density perturbations in the decretion disc due to tidal interactions with the NS (L. Ducci et al. 2016; A. F. Rajoelimanana et al. 2017).

On longer time-scales, photometry revealed a ∼420-d *super-orbital* optical modulation, which could be caused by the build-up and depletion of a high-inclination decretion disc, which toggles the system between different states of activity (C. Alcock et al. 2001; K. E. McGowan & P. A. Charles 2003; A. F. Rajoelimanana et al. 2017). Under this interpretation, during *active/flaring* phases, the system is optically fainter because the disc partially occults the B star – consistent with Balmer (and occasional He I) emission lines and reddening – while accretion as the NS crosses the disc triggers X-ray and optical flares. Successive periastron passages may deplete the disc, producing *quiescent* intervals when the optical emission is relatively stable and at its brightest, dominated by the naked B star. However, weak orbital outbursts sometimes persist, and since about 2010, the quiescent phases have shortened, suggesting that the disc is more persistently present (P. C. Schmidtke, A. P. Cowley & A. Udalski 2014; L. Ducci et al. 2016, 2022; A. F. Rajoelimanana et al. 2017). Alternatively, the superorbital modulation may arise from precession of the decretion disc (R. G. Martin & P. A. Charles 2024).

In Sections 2.1 and 2.2, we present the detection of the radio counterpart to A0538−66 and our subsequent weekly radio monitoring campaign. Sections 2.3 and 2.4 describe our analysis of quasi-simultaneous X-ray and optical data, respectively. Finally, in Section 3, we discuss possible origins of the radio emission, deferring a more detailed analysis to a forthcoming paper once additional multiwavelength data have been obtained.

We define phase zero as the optical maximum, adopting the ephemeris of L. Ducci et al. (2022) ($P_{\rm orb} = 16.64002 \pm 0.00026$ d, $T_0 = {\rm MJD}\ 55673.71 \pm 0.05$), which aligns better with our optical peak than that of A. F. Rajoelimanana et al. (2017). The phase-folded light curves are centred on T_0, such that $-0.5 < \phi \leq 0.0$ and $0.0 < \phi \leq 0.5$ correspond to the half-orbits preceding and following the optical maximum, respectively. From radial-velocity fits, A. F. Rajoelimanana et al. (2017) placed periastron at $\phi_{\rm peri} \approx 0.04$, i.e. ∼0.7 d after the optical maximum, although no revised estimates are available.

2 DATA ANALYSIS

2.1 ASKAP discovery

We discovered radio emission from A0538−66 using data from the Variables and Slow Transients Survey (VAST; T. Murphy et al. 2013) on the Australian Square Kilometre Array Pathfinder (ASKAP; A. W. Hotan et al. 2021), which comprises thirty-six 12-m dishes in Western Australia. VAST observes 40 fields in the Galactic plane and two in the Magellanic Clouds at roughly fortnightly cadence (T. Murphy et al. 2021), achieving typical sensitivities of ∼250 μJy beam^{-1} across the full survey footprint. The data were processed with ASKAPSOFT (T. Cornwell et al. 2011) to produce calibrated visibilities and full-Stokes images, after which catalogues of noise maps and total intensities were generated with SELAVY (M. Whiting & B. Humphreys 2012). The VAST pipeline (A. Stewart et al. 2024) uses these data products and source catalogues to perform source detection, association, and forced photometry, producing a set of light curves that become accessible via a web interface and the VAST-TOOLS PYTHON package (A. Stewart et al. 2025).

A0538−66 was detected in data from the VAST pilot Galactic surveys (2022–2024) using a machine-learning-based anomaly programme, which identified its light curve as highly anomalous

[2]Some super-Eddington outbursts may have been missed or confused in all-sky survey data because A0538−66 lies only ∼30 arcmin from the luminous LMC X-4, and its bright episodes are typically short.
[3]SAX J0635.2+0533 is reported to have a shorter period, but is more likely rotation powered (N. La Palombara & S. Mereghetti 2017).

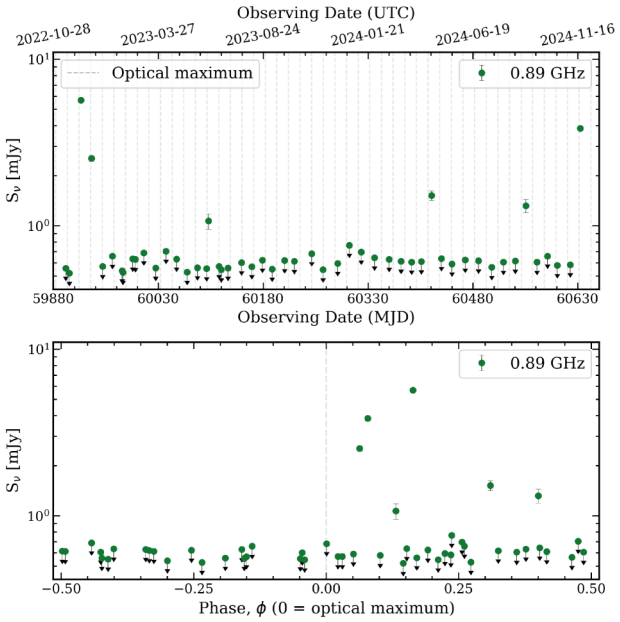

Figure 1. 888 MHz flux densities (top) and phase-folded light curve (bottom) from the VAST survey on ASKAP. Grey lines mark the dates of the optical maxima, arrows denote $3\sigma_{\rm rms}$ upper limits (where $\sigma_{\rm rms}$ is the image root-mean-square noise), and error bars show the 1σ statistical uncertainties.

(A. Andersson et al. 2025; Andersson et al., in preparation). The search used code adapted from ASTRONOMALY (M. Lochner & B. A. Bassett 2021), which computes features for each light curve and applies anomaly-detection algorithms to assign an anomaly score. Sources are then presented to users via an interface that iteratively reranks them to reflect the required scientific goals (active learning). Independently, A0538−66 was detected with an XRB monitoring programme, which conducted a pilot census of XRB variability during the surveys (Qiu et al., in preparation).

The VAST light curve for A0538−66, spanning 2022 November 14 (MJD 59897) to 2024 November 19 (MJD 60633), is shown in Fig. 1. The source was detected multiple times, notably peaking at ∼6 mJy in 2022 December – a few weeks after renewed activity was reported (R. Stubbings & G. Skinner 2022) – and rebrightening to ∼4 mJy in the final 2024 November epoch. The plot for the phase-folded flux densities (lower panel) shows that all the strong radio flares occurred within the ∼0.2 phase following the optical maximum, likely around (and shortly after) periastron passage.

2.2 MeerKAT

Subsequent to its radio detection, we followed up with observations of A0538−66 through the X-KAT programme – the successor of ThunderKAT (P. Woudt et al. 2018) – which conducts weekly radio monitoring of active XRBs with the MeerKAT telescope in South Africa (J. Jonas & the MeerKAT Team 2018). The array comprises sixty-four 13.5-m dishes, and is equipped with L-, S-, and UHF-band receivers. It has a dense core and a maximum baseline of ∼8 km, providing excellent snapshot *uv* coverage. In the L band (0.856–1.712 GHz; centred at 1.284 GHz, with a 856 MHz bandwidth), it covers a large field of view of 1.69 deg^2, and achieves a resolution of ∼5 arcsec.

2.2.1 Calibration and imaging

MeerKAT's higher sensitivity compared to ASKAP allowed us to probe much lower flux densities for A0538−66. Our first L-band observation on 2025 February 4 (MJD 60710) detected an unresolved ∼0.2 mJy source at its reported position. We then monitored the target at L band at roughly weekly cadence until 2025 October 12 (MJD 60960), yielding a total of 35 epochs – one of which (ID 1742666474) was excluded from our analysis due to calibration issues.

During each epoch, the bright and compact active galactic nucleus (AGN) J0408−6545/PKS 0408−65 was used as the primary (i.e. delay, bandpass, and flux density), secondary (i.e. complex gain), and leakage calibrator, while the strongly polarized AGN J0521+1638/3C138 was used as the cross-hand phase calibrator. Each block consisted of the sequence: (J0408−6545: 5 min), (A0538−66: 15 min), (J0408−6545: 5 min), (J0521+1638: 10 min).

The data were processed using the semi-automated routine POLKAT (A. K. Hughes et al. 2025a). Using this pipeline, the visibilities were first frequency averaged to 1024 channels. Initial flagging and reference calibration were then performed with CASA (CASA Team 2022) using the calibrator fields. The target data were further flagged with TRICOLOUR (B. V. Hugo et al. 2022), and an initial image was produced with WSCLEAN (A. R. Offringa et al. 2014). A mask generated with BREIZORRO (A. J. Ramaila, O. Smirnov & I. Heywood 2023) was applied for a first masked deconvolution, and the resulting model was used for direction-independent self-calibration with QUARTICAL (J. S. Kenyon et al. 2025). A second masked deconvolution of the self-calibrated visibilities produced 16 channelized images, and a high-sensitivity multifrequency synthesis (MFS) image. We adopted a Briggs robustness parameter (D. S. Briggs 1995) of 0 to optimize sensitivity while mitigating non-Gaussian features in the synthesized beam that arise at high Briggs weightings.

2.2.2 Analysis

The root-mean-square noise ($\equiv\sigma_{\rm rms}$) in each MFS image was measured in a source-free 4 arcmin^2 region near the target, using the CASA task `imstat`, yielding typical values of ∼20 μJy beam^{-1}. The source was detected (peak flux density $>3\sigma_{\rm rms}$) in every epoch and was unresolved. Flux densities were obtained with `imfit` by fitting an elliptical Gaussian whose shape was fixed to the synthesized beam (i.e. a point-source model), using a small region centred on the source. The results are shown in Fig. 2(a), with error bars indicating the 1σ uncertainties from the fits (an additional ∼5–10 per cent systematic uncertainty is recommended). In the corresponding phase-folded plot in Fig. 3(a), the light blue shading shows the average flux densities in ∼0.8-d bins.

We computed intraband spectral indices only for epochs with peak MFS target flux densities that are $\gtrsim 30\sigma_{\rm rms}$, to avoid biases introduced when low signal-to-noise ratio data are used (I. Heywood et al. 2016). For each of these epochs, the 16 subband flux densities (S_ν) were fit as a function of frequency (ν) using a power-law model ($S_\nu \propto \nu^\alpha$, where α is the spectral index). To achieve this, the data along each axis were log-transformed, and a PYTHON implementation of LINMIX (B. C. Kelly 2007) was employed, which performs Markov chain Monte Carlo simulations to fit a linear model, accounting for measurement uncertainties, upper limits in the dependent variable, and intrinsic scat-

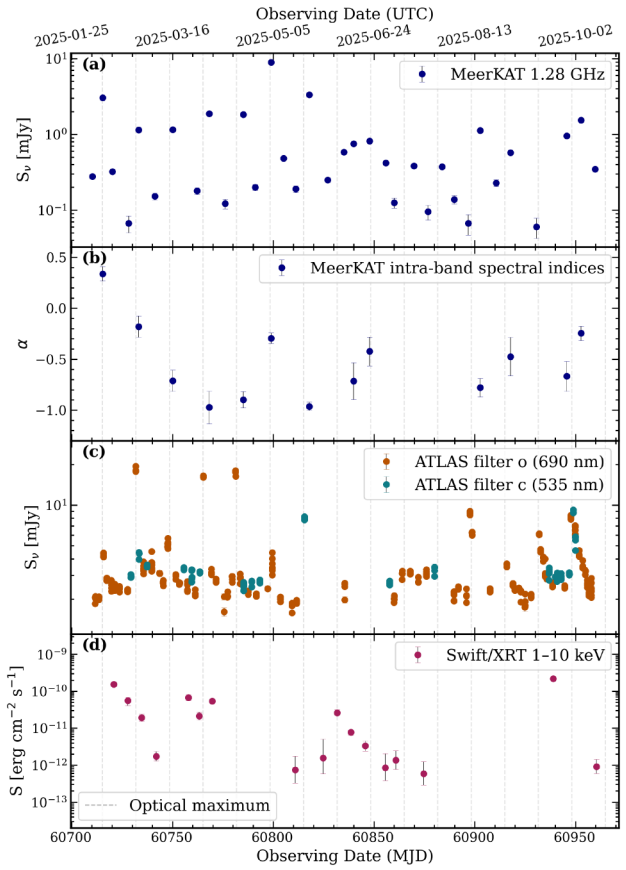

Figure 2. (a) 1.28 GHz MeerKAT radio core flux densities and (b) intraband spectral indices. (c) ATLAS filter o (560–820 nm) and c (420–650 nm) flux densities. (d) *Swift*/XRT unabsorbed 1–10 keV fluxes. Grey lines indicate optical maxima, and error bars show 1σ statistical uncertainties.

ter. Given that we report only the brightest epochs (which yield detections in all subbands), we also used a simple closed-form weighted least-squares fit, obtaining slopes (i.e. estimates of α) that are consistent within uncertainties.

We did not detect any significant polarized emission spatially coincident with the Stokes I source. Using the brightest epoch (2025 May 4; MJD 60809; $I = 8.78 \pm 0.02$ mJy), we extracted Stokes V and linear polarization flux densities $\left(P = \sqrt{Q^2 + U^2}\right)$ by performing beam-shaped forced aperture photometry fixed at the Stokes I position. From these flux densities, we derived a 3σ confidence interval on the circular polarization fraction of $-0.5\,\text{per cent} < m_c \equiv V/I < 0.4\,\text{per cent}$, and a one-sided $\approx 3\sigma$ upper limit on the linear polarization fraction of $m_l \equiv P/I < 1.1$ per cent, following the Ricean statistical approach of J. E. Vaillancourt (2006). Since image-plane methods are susceptible to bandwidth depolarization, we reimaged the epoch with 1024 frequency channels and applied rotation measure (RM) synthesis using RM-TOOLS (M. A. Brentjens & A. G. de Bruyn 2005; C. R. Purcell et al. 2020). At this level of channelization, we are unaffected by bandwidth depolarization for $|\text{RM}| \lesssim 10^4\,\text{rad m}^{-2}$. The resulting Faraday dispersion function shows a marginal peak at $\text{RM} \approx 1600\,\text{rad m}^{-2}$ with a Gaussian-equivalent significance of 2.3σ (C. A. Hales et al. 2012), and yields the same constraint on m_l as the image-plane analysis. This RM is approximately an order of magnitude larger than typical pulsar values in the Magellanic Clouds ($|\text{RM}| \lesssim 100\,\text{rad m}^{-2}$; e.g.

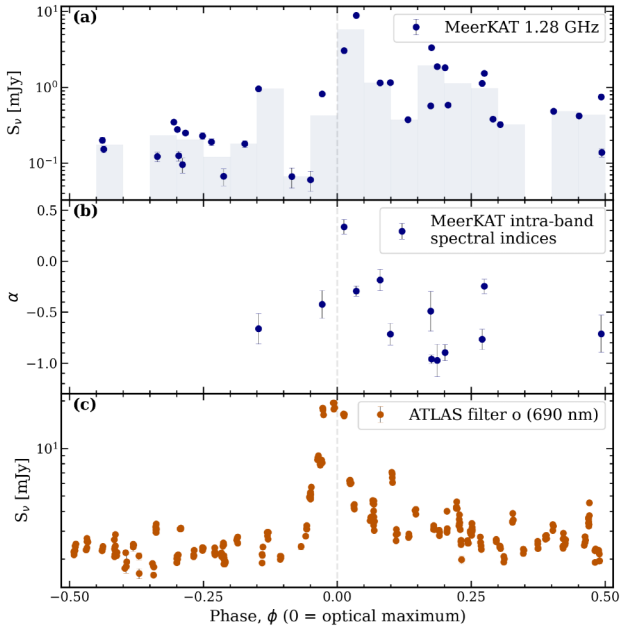

Figure 3. Phase-folded 1.28 GHz MeerKAT (a) flux densities and (b) intraband spectral indices. (c) ATLAS filter o (560–820 nm) data, over the date range MJDs = [60710, 60961] (covering multiple orbital cycles), where phase zero is the optical maximum. The light blue shading in panel (a) shows average data in ∼0.8-d bins. Phase-folded *Swift*/XRT data are not shown, as they do not appear to be orbitally modulated.

S. Johnston et al. 2022), which supports the interpretation that the signal is spurious. Consequently, we favour the interpretation that A0538−66 is weakly polarized, although whether this is intrinsic or the result of depolarization by various factors (e.g. A. Pasetto et al. 2018; A. P. Marscher & S. G. Jorstad 2021; A. K. Hughes et al. 2023; M. Chernyakova et al. 2024; M. C. Baglio et al. 2025) remains uncertain and will be investigated in future analyses of the polarization properties across all epochs.

We also produced an ∼8.5-h deep image of the field of A0538−66 ($\sigma_{\text{rms}} \sim 10\,\mu\text{Jy beam}^{-1}$), but did not detect its natal supernova remnant (SNR). Indeed, the source has been associated with the LMC open cluster NGC 2034, implying an age $\gtrsim 10^6$ yr (M. Pakull & A. Parmar 1981), in which case its natal SNR (which is expected to fade on $\lesssim 10^5$-yr time-scales; e.g. D. A. Leahy, F. Merrick & M. Filipović 2022) would not be detectable.

2.3 *Swift*/XRT

X-KAT runs in conjunction with the *Swift*KAT programme, which obtained quasi-simultaneous 0.2–10 keV observations of A0538−66 with the *Neil Gehrels Swift Observatory*/X-ray Telescope (*Swift*/XRT; N. Gehrels et al. 2004; D. N. Burrows et al. 2005). The spectra were extracted using the SWIFTTOOLS product generator (P. A. Evans et al. 2007, 2009), which applies the latest software and calibration files. Spectral fitting was performed with XSPEC (K. A. Arnaud 1996) over the range 0.5–10 keV, ignoring bad channels and using Cash statistics (`cstat` ; W. Cash 1979) after data were grouped to have at least one count per bin. Since our aim is to qualitatively track the X-ray flux evolution during our radio campaign, we adopted a simple fitting routine, reserving a more detailed analysis for future work. We extracted unabsorbed 1–10 keV fluxes following the approach of previous studies (e.g. L. Ducci et al. 2019b), adopting `tbabs*(pegpwrlw)`

for low-count spectra (<50 counts), and the phenomenological model `tbabs*(pegpwrlw + pegpwrlw)` to capture the spectral features at both high and low energies in the higher count spectra. For `tbabs` – parametrized by the line-of-sight column density $N_{\rm H}$ – we used Wilm abundances (J. Wilms, A. Allen & R. McCray 2000) and Vern cross-sections (D. A. Verner et al. 1996). Since our spectra are mostly low count (thus $N_{\rm H}$ is poorly constrained), we fixed $N_{\rm H} = 8 \times 10^{20}\,{\rm cm}^{-2}$, but note that varying its value across the range reported in the literature (e.g. L. Ducci et al. 2019b; L. Ducci & S. Mereghetti 2025; M. Rigoselli et al. 2025) does not significantly affect our results. Uncertainties were extracted using the `error` command at the 1σ level, and the results are shown in Fig. 2(d).

2.4 ATLAS

The Asteroid Terrestrial-impact Last Alert System (ATLAS; J. L. Tonry et al. 2018) consists of four telescopes and can survey the entire visible sky multiple times a day. Although it was designed to detect potentially hazardous near-Earth objects, its data are valuable for transient sources. We used ATLAS measurements of A0538−66 in the orange (o; 560–820 nm) and cyan (c; 420–650 nm) bands, generated with target-image photometry via the ATLAS server (L. Shingles et al. 2021). Fig. 2(c) shows the ATLAS light curve during our MeerKAT campaign (MJDs 60710–60961), and Fig. 3(c) presents the same data folded on the orbital period.

3 DISCUSSION

As seen in Fig. 3(a), the radio emission of A0538−66 appears to be orbitally modulated – with a peak occurring after the optical maximum, near periastron – and is generally higher after the peak ($0.05 < \phi \leq 0.5$) than before ($-0.5 < \phi \leq -0.05$). However, the behaviour is clearly complex, and the flux density at a particular point in time may be the superposition of various factors such as the orbital (and superorbital) phase and accretion rate. Notably, the ∼1 mJy epoch at $\phi \sim -0.15$ occurred on 2025 September 28 (MJD 60581), just ∼2 d before the super-Eddington X-ray observation reported by L. Ducci et al. (2025), and appears brighter than data points at similar phases. Additionally, from Fig. 3(b), we see a slight tendency for the radio emission to be more optically thick ($\alpha \gtrsim -0.5$) near periastron – although more data are needed to be certain, as we report on very few intraband spectral indices far from periastron because of generally low signal-to-noise ratios at these phases.

It is worth noting that the TRAPUM (TRAnsients and PUlsars with MeerKAT) Large Survey Project (V. Prayag et al. 2024) did not detect any pulsed radio emission from A0538−66 during a 2-h observation on 2024 March 2 (MJD 60371; $\phi \sim 0.3$), ∼5 d after its optical maximum (V. Prayag et al. 2026). Our nearest ASKAP observation, taken ∼6 d later (near apastron) yielded a $3\sigma_{\rm rms}$ upper limit of ∼0.6 mJy.

Furthermore, the optical flaring seen in Fig. 2(c) indicates that the source is in an *active* phase during our monitoring period. In particular, Fig. 3(c) shows that near periastron, an initial strong optical peak occurs, followed by additional flaring. This suggests efficient accretion near periastron if the emission is indeed dominated by reprocessed X-rays (L. Ducci et al. 2019a).

However, Fig. 2(d) shows no sign of the X-ray flux being orbitally modulated (in fact, it shows large variability at the same phase), and that there is no correlation between the radio and X-ray emission. This may partly be due to our sparse sampling and lack of X-ray coverage within ∼1 d of periastron. Additionally, the source has previously exhibited X-ray flares far from periastron passages (see fig. 5 in L. Ducci et al. 2022), and bright X-ray outbursts can last several days (unlike the more localized optical peaks). Dense, quasi-simultaneous radio and X-ray monitoring are required to further investigate the complex behaviour of A0538−66.

3.1 Radio emission mechanisms

In this section, we consider several mechanisms that could produce radio emission in Be/XRBs, but note that the discussion is not exhaustive.

Thermal free–free emission from an ionized stellar wind is possible (N. Panagia & M. Felli 1975; A. E. Wright & M. J. Barlow 1975), although it typically produces positive spectral indices, contrary to most of our observations. Moreover, the emission is classically predicted to scale with the wind mass-loss rate as $S_\nu \propto \dot{M}^{4/3}$, so detectable L-band emission at 50 kpc likely requires $\dot{M} \gtrsim 10^{-4}\,{\rm M}_\odot\,{\rm yr}^{-1}$, far above the $\dot{M} \lesssim 10^{-9}\,{\rm M}_\odot\,{\rm yr}^{-1}$ typical of classical Be stars (J. Krtička 2014).

A more plausible interpretation is *synchrotron* emission. Under the assumption that the peak near periastron is due to synchrotron self-absorption (SSA; H. der Laan 1966), we can obtain *order-of-magnitude* estimates of the properties of the emitting region, using the equations in R. Fender & J. Bright (2019) and Cowie & Fender (in preparation) (assuming electrons with an energy index $p = 2$ and Lorentz factors 3–1000). The SSA assumption is motivated by the observation of an inverted (i.e. positive) spectral index, and by similar behaviour observed in other flaring XRBs (e.g. D. E. Calvelo et al. 2012). Using our peak flux density (∼9 mJy), the source distance, and observing frequency, we estimate a minimum energy of $\sim 2 \times 10^{41}$ erg, an emitting region size of $\sim 2 \times 10^{14}$ cm, and an equipartition magnetic field of ∼0.2 G. For comparison, this minimum flare energy is about two orders of magnitude higher than that of the ∼4 mJy flare from the NS LMXB XTE J1701−462 during an outburst that covered a similar range in X-ray luminosities (K. V. S. Gasealahwe et al. 2024; $D \approx 8.8$ kpc). Assuming that A0538−66 exhibits a radio flare every periastron (supported by our light curve), the lower limit for the power required to produce the radio emission is $\sim 10^{35}\,{\rm erg\,s}^{-1} \approx 10^{-3} L_{\rm Edd}$. Even if the peak is not due to SSA – but is still produced by a power-law population of synchrotron-emitting electrons (whatever the geometry) – the minimum energy and power constraints remain valid, and the emitting region size becomes a lower limit. Bulk relativistic motion of the radio-emitting region could alter these estimates, but for a large range of parameter space, the energy remains a lower limit (R. Fender & J. Bright 2019). Additionally, changes in the line of sight or the velocity of bulk relativistic motion could explain the observed scatter in the light curve.

The synchrotron emission could originate from *relativistic jets or ejecta*, as commonly seen in LMXBs (R. Fender 2006). This mechanism has also been proposed for Be/XRBs – first for Swift J0243.6+6124 (J. den Eijnden et al. 2018, 2019), and more recently for 1A 0535+262 (J. den Eijnden et al. 2022) and LS V +44 17 (J. den Eijnden et al. 2024). The predominantly optically thin spectral index of A0538−66 suggests emission from discrete, short-lived ejecta rather than a steady compact jet, and the jet axis could be precessing as seen in Circinus X-1 (Cir X-1; F. J. Cowie et al. 2025).

Alternatively, the synchrotron emission could originate from shocks between a *pulsar wind* and the Be companion's stellar wind or decretion disc, as inferred in γ-ray binaries (see G. Dubus 2013 for a review) such as PSR B1259−63 (M. Tavani & J. Arons 1997; S. Johnston et al. 2005). Another possibility is that it arises due to outflows powered by a magnetospheric *propeller* mechanism (A. F. Illarionov & R. A. Sunyaev 1975; M. M. Romanova et al. 2005).

The emission mechanism that is operating depends on the relative positions of three radii:

(i) light-cylinder radius $R_{\rm lc} \simeq 4.8 \times 10^9 P_{\rm s}\,{\rm cm} = 3.3 \times 10^8$ cm;
(ii) corotation radius $R_{\rm co} \simeq 1.68 \times 10^8\, M_{1.4}^{1/3} P_{\rm s}^{2/3}$ cm $= 2.8 \times 10^7$ cm;
(iii) magnetospheric radius $R_{\rm m} \simeq 2.5 \times 10^8 k M_{1.4}^{1/7} R_6^{10/7} B_{12}^{4/7} L_{37}^{-2/7}$ cm;

where $P_{\rm s}$ is the spin period in seconds, and the NS mass, radius, surface magnetic field, and luminosity are respectively scaled as $M = M_{1.4} 1.4\,{\rm M}_\odot$, $R = R_6 10^6$ cm, $B = B_{12} 10^{12}$ G, and $L = L_{37} 10^{37}$ erg s^{-1} (we use $R_6 = 1, M_{1.4} = 1$). Note that the location of $R_{\rm m}$ is quite uncertain; we use S. S. Tsygankov et al. (2017) equation 2, and assume $k = 0.5$ for disc accretion, although L. Ducci et al. (2019b) suggested that A0538−66 may sometimes be in a regime of spherical accretion. The source is in a direct-accretion regime when $R_{\rm m} < R_{\rm co}$, a propeller outflow occurs when $R_{\rm lc} > R_{\rm m} > R_{\rm co}$, and an intrabinary shock can form when $R_{\rm m} > R_{\rm lc}$ (respectively cases A/B, C, and D in the simulations by K. Parfrey & A. Tchekhovskoy 2017).

L. Ducci & S. Mereghetti (2025) considered two scenarios to explain the presence of X-ray pulsations in A0538−66 at $L_{\rm X_0} \sim 8 \times 10^{36}$ erg s^{-1}. In the *first scenario*, the NS is directly accreting at $L_{\rm X_0}$, implying $B < 7 \times 10^{10}$ G, which would be unusually low for an NS HMXB (see discussion in L. Ducci & S. Mereghetti 2025). In this case, the source would be in either the propeller or direct-accretion regimes during all epochs in our campaign, so the radio emission likely arises from a propeller outflow or jet ejecta.

In the *second scenario*, the NS resides in a propeller phase at $L_{\rm X_0}$ – so can have a stronger magnetic field of $B < 5 \times 10^{12}$ G (using $R_{\rm lc} > R_{\rm m}$) – and pulsations arise when gas intermittently overcomes the magnetospheric barrier and accretes onto the NS poles (in between cases B and C in K. Parfrey & A. Tchekhovskoy 2017). In this case, the source could transition between the propeller and pulsar-wind shock regimes at some $L_{\rm X} < L_{\rm X_0}$ that depends on the exact magnetic field strength (i.e. a 'flip-flop' scenario, as proposed for the γ-ray binary LS I +61°303; D. F. Torres et al. 2012). We note that for $B < 5 \times 10^{11}$ G, this transition would fall below the lowest X-ray flux seen in our *Swift*/XRT monitoring, which would again suggest that all radio emission originates in an accretion-flow-dominated state. It is unclear whether two different radio emission mechanisms alternate in A0538−66, as we do not observe a clear dichotomy in the radio properties (e.g. luminosity and spectral index) above and below a certain $L_{\rm X}$. If a subset of the radio observations (those at low $L_{\rm X}$) originate from a shock between the pulsar wind and the Be-star's disc, the field $B < 5 \times 10^{12}$ G implies a pulsar spin-down power of $\dot{E} \lesssim 10^{37}$ erg s^{-1}, which gives a ratio of radio luminosity to $\dot{E}$ that is comparable to those in two systems with intrabinary shocks and known $\dot{E}$, namely PSR B1259−63 (S. Johnston et al. 1992, 1996; G. Dubus 2013; M. Chernyakova et al. 2024) and PSR J2032+4127 (F. Camilo et al. 2009; A. G. Lyne et al. 2015; W. C. G. Ho et al. 2017; C.-Y. Ng et al. 2019). These systems have much wider orbits than A0538−66 (respectively $P_{\rm orb} \approx 3.4$ yr and ≈ 45−50 yr); thus, far from periastron, the companion-wind density at the NS is low enough for radio pulsations to be active and detectable – a situation not observed to date in A0538−66.

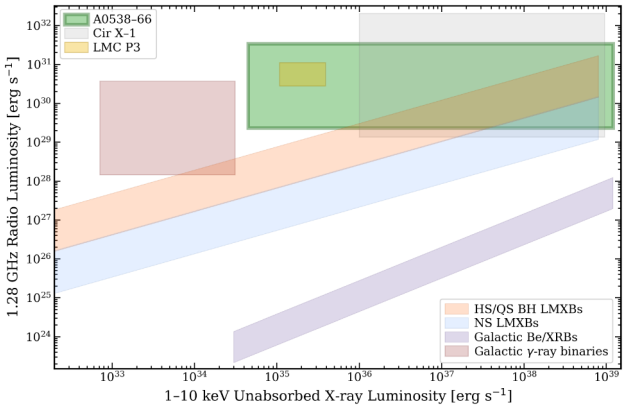

Figure 4. A schematic showing regions in radio–X-ray parameter space occupied by different types of systems (see the text for caveats). Orange and blue, respectively, indicate the hard/quiescent-state BH and NS LMXBs. Purple and red show subsets of the Galactic Be/X-ray binary and γ-ray binary classes, respectively, while yellow indicates the extra-Galactic γ-ray binary LMC P3. A0538−66 and Cir X-1 are shown in green and grey, respectively.

3.2 Broader context

Fig. 4 shows a schematic comparison of quasi-simultaneous unabsorbed 1–10 keV X-ray luminosities ($L_{\rm X}$) and 1.28 GHz radio luminosities scaled by frequency ($L_{\rm R} = \nu L_\nu$) for X-ray and γ-ray binaries. The diagram is deliberately simplified and – given sensitivity limits and sparse sampling – may not capture the full parameter space of each population, but it provides a useful high-level comparison of A0538−66 with other similar systems. The green shading indicates the $L_{\rm R}$–$L_{\rm X}$ parameter space occupied by A0538−66, though $L_{\rm X}$ may extend down to even lower values in quiescence (P. Kretschmar et al. 2004). Orange and blue show the regions corresponding to the canonical hard/quiescent BH LMXB track and to NS LMXB detections, respectively (e.g. E. Gallo, N. Degenaar & J. van den Eijnden 2018). In reality, these regions overlap: many BH LMXBs extend to lower $L_{\rm R}$ (e.g. A. K. Hughes et al. 2025b), and NS LMXBs exhibit diverse behaviour (e.g. A. J. Tetarenko et al. 2016; V. Tudor et al. 2017). Additionally, many NS observations are upper limits, so this region likely extends to even lower $L_{\rm R}$ than currently detectable.

Using observations of 1A 0535+262, SAX J2103.5+4545, an outburst of Swift J0243.6+6124, and a giant outburst of GRO J1008−57, J. den Eijnden et al. (2022) proposed that *Galactic Be/XRBs* display correlated radio and X-ray emission – consistent with radio emission arising from accretion-driven compact jets – contrary to our (sparse) A0538−66 observations. These authors further suggested that this group (shown in purple in Fig. 4) has a lower $L_{\rm R}/L_{\rm X}$ normalization than NS LMXBs. Thus, regardless of whether the radio emission is jet-driven or has another origin (e.g. M. Chatzis, M. Petropoulou & G. Vasilopoulos 2022), Be/XRBs at comparable luminosities would not be detectable at the LMC distance – highlighting how luminous A0538−66 is. An investigation into whether this difference may be related to A0538−66's significantly shorter spin period compared to other Be/XRBs (see M. Rigoselli et al. 2025, fig. 7) is worthwhile.

As first noted by P. Murdin, G. Branduardi-Raymont & A. N. Parmar (1981), A0538−66 resembles the NS LMXB Cir X-1 in terms of its ∼16.6-d orb ital period (L. J. Kaluzienski et al. 1976) and X-ray light curve, although Cir X-1 is far younger (<4600 yr; S. Heinz et al. 2013). Cir X-1 typically shows radio flux densities of the order ∼10 mJy, which (at $D \approx 9.4$ kpc; S. Heinz et al. 2015) corresponds to luminosities that are comparable to A0538−66. However, it occasionally flares to $\gtrsim$1 Jy (R. P. Armstrong et al. 2013), about an order of magnitude more luminous than A0538−66's peak (observed to date). In grey in Fig. 4, we plot a representative orbitally averaged range of L_X for Cir X-1; while it has exhibited lower L_X dips near periastron, these are likely due to absorption rather than a decrease in the accretion rate (A. D'Aì et al. 2012; N. S. Schulz et al. 2020). Cir X-1 has long been regarded as an extreme outlier among NS XRBs, so our finding that A0538−66 resides in a similar region of L_R–L_X space is particularly intriguing.

In red in Fig. 4, we indicate the approximate location of some of the most luminous *Galactic γ-ray binaries* – 1FGL J1018.6−5856 (1FGL J1018; B. Soelen et al. 2022; $D \approx 4.4$ kpc), LS I +61°303 (P. Esposito et al. 2007; M. Massi & M. Kaufman Bernadó 2009; L. Zimmermann, L. Fuhrmann & M. Massi 2015; M. Massi & G. Torricelli-Ciamponi 2016; M. Massi, S. Migliari & M. Chernyakova 2017; $D \approx 2.6$ kpc), LS 5039 (V. Bosch-Ramon et al. 2005; B. Marcote et al. 2015; I. Volkov et al. 2021; $D \approx 2.0$ kpc), PSR B1259−63 (M. Chernyakova et al. 2009; $D \approx 2.4$ kpc), and 4FGL J1405.1−6119 (R. H. D. Corbet et al. 2019; $D \approx 7.7$ kpc) – but note that there may be fainter sources within this group (e.g. PSR J2032+4127; W. C. G. Ho et al. 2017; C.-Y. Ng et al. 2019; M. Chernyakova et al. 2020; $D \approx 1.4$ kpc). Interestingly, 1FGL J1018 also has $P_{orb} \approx 16.6$ d (B. Soelen et al. 2022); however, its most luminous L-band MeerKAT epoch (to date) is comparable to the least luminous A0538−66 epochs (Mathiba et al., in preparation). In addition, the yellow region in Fig. 4 shows the approximate parameter space occupied by the only confirmed *extra-Galactic γ-ray binary*, LMC P3 (R. H. D. Corbet et al. 2016), whose L-band MeerKAT flux density peaks at slightly lower but comparable values to A0538−66 (namely $\lesssim$3 mJy; Mathiba et al., in preparation).

Clearly, A0538−66 straddles the region in L_R–L_X parameter space between γ-ray binaries and outlier NS LMXB systems like Cir X-1.

4 CONCLUSIONS

A0538−66 is a Be/XRB in the LMC that exhibits a range of unusual properties. We detected the source at radio wavelengths for the first time in 0.89 GHz ASKAP data. We subsequently conducted a weekly 1.28 GHz MeerKAT monitoring campaign, during which it was consistently detected and reached a peak flux density of ∼9 mJy. In addition, we found tentative evidence that the radio emission is orbitally modulated. In upcoming work, we will present the results from a high-cadence multiwavelength campaign aimed at understanding the origins of emission in this peculiar system.

DATA AVAILABILITY

The code used to generate the plots in this paper is available at https://github.com/JustineCrook/A0538-66_analysis; any updates to the radio and X-ray results will be shared here. Data from MeerKAT are available through the SARAO data archive (Proposal ID: SCI-20230907-RF-01): https://archive.sarao.ac.za/. Data from ATLAS are available at https://fallingstar-data.com/forcedphot/. Data from the *Swift*/XRT are publicly available through the *Swift* archive: https://www.swift.ac.uk/swift_portal.

For the MeerKAT data reduction, we made use of POLKAT: https://github.com/AKHughes1994/polkat. When fitting the MeerKAT intraband spectral indices, we used the PYTHON implementation of LINMIX from https://github.com/jmeyers314/linmix.

ACKNOWLEDGEMENTS

JC-M acknowledges financial support from the Rhodes Trust at the University of Oxford. RF acknowledges support from the European Research Council (ERC) Synergy Grant 'Blackholistic', UK Research and Innovation (UKRI), and the Hintze Family Charitable Foundation. JvdE was supported by funding from the European Union's Horizon Europe research and innovation programme under the Marie Skłodowska-Curie grant agreement no. 101148693 (MeerSHOCKS). DLK was supported by NSF grant AST-2511757. Parts of this research were conducted by the Australian Research Council Centre of Excellence for Gravitational Wave Discovery (OzGrav), project number CE230100016. LD acknowledges funding from the Deutsche Forschungsgemeinschaft (DFG, German Research Foundation) – project number 549824807. PC acknowledges the Leverhulm Trust for an Emeritus Fellowship.

The MeerKAT telescope is operated by the South African Radio Astronomy Observatory, which is a facility of the National Research Foundation, an agency of the Department of Science and Innovation. The authors would like to thank Lilia Tremou, Andrew Hughes, Francesco Carotenuto, and Payaswini Saikia for scheduling the MeerKAT observations. We acknowledge the use of the Inter-University Institute for Data Intensive Astronomy (IDIA) data-intensive research cloud for data processing. IDIA is a South African University partnership involving the University of Cape Town, the University of Pretoria, and the University of the Western Cape.

This scientific work uses data obtained from Inyarrimanha Ilgari Bundara, the CSIRO Murchison Radio-astronomy Observatory. We acknowledge the Wajarri Yamaji People as the Traditional Owners and native title holders of the Observatory site. CSIRO's ASKAP radio telescope is part of the Australia Telescope National Facility (https://ror.org/05qajvd42). Operation of ASKAP is funded by the Australian Government with support from the National Collaborative Research Infrastructure Strategy. ASKAP uses the resources of the Pawsey Supercomputing Research Centre. Establishment of ASKAP, Inyarrimanha Ilgari Bundara, the CSIRO Murchison Radio-astronomy Observatory, and the Pawsey Supercomputing Research Centre are initiatives of the Australian Government, with support from the Government of Western Australia and the Science and Industry Endowment Fund.

This research was supported by the Sydney Informatics Hub (SIH), a core research facility at The University of Sydney. This work was also supported by software support resources awarded under the Astronomy Data and Computing Services (ADACS) Merit Allocation Program. ADACS is funded from the Astronomy National Collaborative Research Infrastructure Strategy (NCRIS) allocation provided by the Australian Government and managed by Astronomy Australia Limited (AAL).

REFERENCES

Alcock C. et al., 2001, MNRAS, 321, 678
Andersson A. et al., 2025, MNRAS, 538, 1397
Armstrong R. P. et al., 2013, MNRAS, 433, 1951
Arnaud K. A., 1996, in Jacoby G. H., Barnes J., eds, ASP Conf. Ser. Vol. 101, Astronomical Data Analysis Software and Systems V. Astron. Soc. Pac., San Francisco, p. 17
Baglio M. C. et al., 2025, A&A, 694, L19
Bosch-Ramon V., Paredes J. M., Ribó M., Miller J. M., Reig P., Martí J., 2005, ApJ, 628, 388
Brentjens M. A., de Bruyn A. G., 2005, A&A, 441, 1217
Briggs D. S., 1995, Am. Astron. Soc. Meeting, 187, 112.02
Burrows D. N. et al., 2005, Space Sci. Rev., 120, 165
Calvelo D. E., Fender R. P., Tzioumis A. K., Kawai N., Broderick J. W., Bell M. E., 2012, MNRAS, 419, 436
Camilo F. et al., 2009, ApJ, 705, 1
Campana S., Stella L., Israel G. L., Moretti A., Parmar A. N., Orlandini M., 2002, ApJ, 580, 389
CASA Team, 2022, PASP, 134, 114501
Cash W., 1979, ApJ, 228, 939
Chatzis M., Petropoulou M., Vasilopoulos G., 2022, MNRAS, 509, 2532
Chernyakova M., Neronov A., Aharonian F., Uchiyama Y., Takahashi T., 2009, MNRAS, 397, 2123
Chernyakova M., Malyshev D., Blay P., van Soelen B., Tsygankov S., 2020, MNRAS, 495, 365
Chernyakova M., Malyshev D., van Soelen B., Mc Keague S., O'Sullivan S. P., Buckley D., 2024, MNRAS, 528, 5231
Corbet R. H. D. et al., 2016, ApJ, 829, 105
Corbet R. H. D. et al., 2019, ApJ, 884, 93
Cornwell T., Humphreys B., Lenc E., Voronkov M., Whiting M., Mitchell D., Ord S., Collins D., 2011, ASKAP-SW-0020: ASKAP Science Processing. ASKAP Science Case Memo Series 02. Available at: http://www.atnf.csiro.au/projects/askap/ASKAP-SW-0020.pdf
Cowie F. J. et al., 2025, MNRAS, 544, L37
D'Aì A. et al., 2012, A&A, 543, A20
Dubus G., 2013, A&AR, 21, 64
Ducci L., Mereghetti S., 2025, ApJ, 989, 150
Ducci L., Covino S., Doroshenko V., Mereghetti S., Santangelo A., Sasaki M., 2016, A&A, 595, A103
Ducci L., Mereghetti S., Hryniewicz K., Santangelo A., Romano P., 2019a, A&A, 624, A9
Ducci L., Mereghetti S., Santangelo A., 2019b, ApJ, 881, L17
Ducci L. et al., 2022, A&A, 661, A22
Ducci L., Mereghetti S., Bachetti M., 2025, Astron. Telegram, 17455, 1
Esposito P., Caraveo P. A., Pellizzoni A., de Luca A., Gehrels N., Marelli M. A., 2007, A&A, 474, 575
Evans P. A. et al., 2007, A&A, 469, 379
Evans P. A. et al., 2009, MNRAS, 397, 1177
Fender R., 2006, in Lewin W. H. G., van der Klis M., eds, Compact Stellar X-ray Sources. Cambridge Univ. Press, Cambridge, p. 381
Fender R., Bright J., 2019, MNRAS, 489, 4836
Gallo E., Degenaar N., van den Eijnden J., 2018, MNRAS, 478, L132
Gasealahwe K. V. S. et al., 2024, MNRAS, 533, 1800
Gehrels N. et al., 2004, ApJ, 611, 1005
Hales C. A., Gaensler B. M., Norris R. P., Middelberg E., 2012, MNRAS, 424, 2160
Heinz S. et al., 2013, ApJ, 779, 171
Heinz S. et al., 2015, ApJ, 806, 265
Heywood I. et al., 2016, MNRAS, 460, 4433
Ho W. C. G., Ng C.-Y., Lyne A. G., Stappers B. W., Coe M. J., Halpern J. P., Johnson T. J., Steele I. A., 2017, MNRAS, 464, 1211
Hotan A. W. et al., 2021, Publ. Astron. Soc. Aust., 38, e009
Hughes A. K. et al., 2023, MNRAS, 521, 185
Hughes A. K., Cowie F. J., Heywood I., Hugo B., 2025a, Astrophysics Source Code Library, record ascl:2502.026
Hughes A. K. et al., 2025b, MNRAS, 542, 1803
Hugo B. V., Perkins S., Merry B., Mauch T., Smirnov O. M., 2022, in Ruiz J. E., Pierfedereci F., Teuben P., eds, ASP Conf. Ser. Vol. 532, Astronomical Data Analysis Software and Systems XXX. Astron. Soc. Pac., San Francisco, p. 541
Illarionov A. F., Sunyaev R. A., 1975, A&A, 39, 185
Johnston S., Manchester R. N., Lyne A. G., Bailes M., Kaspi V. M., Qiao G., D'Amico N., 1992, ApJ, 387, L37
Johnston S., Manchester R. N., Lyne A. G., D'Amico N., Bailes M., Gaensler B. M., Nicastro L., 1996, MNRAS, 279, 1026
Johnston S., Ball L., Wang N., Manchester R. N., 2005, MNRAS, 358, 1069
Johnston S. et al., 2022, MNRAS, 509, 5209
Jonas J., the MeerKAT Team, 2018, Proc. Sci., The MeerKAT Radio Telescope. SISSA, Trieste, PoS(MeerKAT2016)001
Kaluzienski L. J., Holt S. S., Boldt E. A., Serlemitsos P. J., 1976, ApJ, 208, L71
Kelly B. C., 2007, ApJ, 665, 1489
Kenyon J. S., Perkins S. J., Bester H. L., Smirnov O. M., Russeeawon C., Hugo B. V., 2025, Astron. Comput., 52, 100962
Kretschmar P., Wilms J., Staubert R., Kreykenbohm I., Heindl W. A., 2004, in Schoenfelder V., Lichti G., Winkler C., eds, 5th INTEGRAL Workshop on the INTEGRAL Universe (ESA SP-552). ESA Publications Division, Noordwijk, p. 329
Krtička J., 2014, A&A, 564, A70
La Palombara N., Mereghetti S., 2017, A&A, 602, A114
Leahy D. A., Merrick F., Filipović M., 2022, Universe, 8, 653
Lochner M., Bassett B. A., 2021, Astron. Comput., 36 100481
Lyne A. G., Stappers B. W., Keith M. J., Ray P. S., Kerr M., Camilo F., Johnson T. J., 2015, MNRAS, 451, 581
McGowan K. E., Charles P. A., 2003, MNRAS, 339, 748
Marcote B., Ribó M., Paredes J. M., Ishwara-Chandra C. H., 2015, MNRAS, 451, 59
Marscher A. P., Jorstad S. G., 2021, Galaxies, 9, 27
Martin R. G., Charles P. A., 2024, MNRAS, 528, L59
Massi M., Kaufman Bernadó M., 2009, ApJ, 702, 1179
Massi M., Torricelli-Ciamponi G., 2016, A&A, 585, A123
Massi M., Migliari S., Chernyakova M., 2017, MNRAS, 468, 3689
Moritani Y. et al., 2013, PASJ, 65, 83
Murdin P., Branduardi-Raymont G., Parmar A. N., 1981, MNRAS, 196, 95P
Murphy T. et al., 2013, Publ. Astron. Soc. Aust., 30, e006
Murphy T. et al., 2021, Publ. Astron. Soc. Aust., 38, e054
Ng C.-Y. et al., 2019, ApJ, 880, 147
Offringa A. R. et al., 2014, MNRAS, 444, 606
Okazaki A. T., Negueruela I., 2001, A&A, 377, 161
Pakull M., Parmar A., 1981, A&A, 102, L1
Panagia N., Felli M., 1975, A&A, 39, 1
Parfrey K., Tchekhovskoy A., 2017, ApJ, 851, L34
Pasetto A., Carrasco-González C., O'Sullivan S., Basu A., Bruni G., Kraus A., Curiel S., Mack K.-H., 2018, A&A, 613, A74
Pietrzyński G. et al., 2019, Nature, 567, 200
Prayag V. et al., 2024, MNRAS, 533, 2570
Prayag V. et al. 2026. MNRAS, 545, staf2193
Purcell C. R., Van Eck C. L., West J., Sun X. H., Gaensler B. M., 2020, Astrophysics Source Code Library, record ascl:2005.003
Rajoelimanana A. F., Charles P. A., Meintjes P. J., Townsend L. J., Schurch M. P. E., Udalski A., 2017, MNRAS, 464, 4133
Ramaila A. J., Smirnov O., Heywood I., 2023, Astrophysics Source Code Library, record ascl:2305.009
Reig P., 2011, Ap&SS, 332, 1
Rigoselli M., Tresoldi C., Ducci L., Mereghetti S., 2025, Astron. Nachr., 346, e20240098
Romanova M. M., Ustyugova G. V., Koldoba A. V., Lovelace R. V. E., 2005, ApJ, 635, L165
Schmidtke P. C., Cowley A. P., Udalski A., 2014, Astron. Telegram, 6135, 1
Schulz N. S., Kallman T. E., Heinz S., Sell P., Jonker P., Brandt W. N., 2020, ApJ, 891, 150

Shingles L. et al., 2021, Transient Name Server, AstroNote 2021-7
Skinner G. K., 1980, Nature, 288, 141
Skinner G. K., Bedford D. K., Elsner R. F., Leahy D., Weisskopf M. C., Grindlay J., 1982, Nature, 297, 568
Stewart A. et al., 2024, askap-vast/vast-pipeline: v1.2.0. Zenodo. Available at: https://doi.org/10.5281/zenodo.13927015
Stewart A., Dobie D., O'Brien A., Kaplan D., 2025, askap-vast/vast-tools: v3.2.0. Zenodo. Available at: https://doi.org/10.5281/zenodo.15363128
Stubbings R., Skinner G., 2022, Astron. Telegram, 15781, 1
Tavani M., Arons J., 1997, ApJ, 477, 439
Tetarenko A. J. et al., 2016, MNRAS, 460, 345
Tonry J. L. et al., 2018, PASP, 130, 064505
Torres D. F., Rea N., Esposito P., Li J., Chen Y., Zhang S., 2012, ApJ, 744, 106
Tsygankov S. S., Mushtukov A. A., Suleimanov V. F., Doroshenko V., Abolmasov P. K., Lutovinov A. A., Poutanen J., 2017, A&A, 608, A17
Tudor V. et al., 2017, MNRAS, 470, 324
Vaillancourt J. E., 2006, PASP, 118, 1340
van den Eijnden J., Degenaar N., Russell T. D., Wijnands R., Miller-Jones J. C. A., Sivakoff G. R., Hernández Santisteban J. V., 2018, Nature, 562, 233
van den Eijnden J., Degenaar N., Russell T. D., Hernández Santisteban J. V., Wijnands R., Miller-Jones J. C. A., Rouco Escorial A., Sivakoff G. R., 2019, MNRAS, 483, 4628
van den Eijnden J., Degenaar N., Russell T. D., Miller-Jones J. C. A., Rouco Escorial A., Wijnands R., Sivakoff G. R., Hernández Santisteban J. V., 2022, MNRAS, 516, 4844
van den Eijnden J. et al., 2024, MNRAS, 527, 4260
van der Laan H., 1966, Nature, 211, 1131
van Soelen B., Mc Keague S., Malyshev D., Chernyakova M., Komin N., Matchett N., Monageng I. M., 2022, MNRAS, 515, 1078
Verner D. A., Ferland G. J., Korista K. T., Yakovlev D. G., 1996, ApJ, 465, 487
Volkov I., Kargaltsev O., Younes G., Hare J., Pavlov G., 2021, ApJ, 915, 61
White N. E., Carpenter G. F., 1978, MNRAS, 183, 11P
Whiting M., Humphreys B., 2012, Publ. Astron. Soc. Aust., 29, 371
Wilms J., Allen A., McCray R., 2000, ApJ, 542, 914
Woudt P. et al., 2018, Proc. Sci., ThunderKAT: The MeerKAT Large Survey Project forImage-Plane Radio Transients. SISSA, Trieste, PoS(MeerKAT2016)013
Wright A. E., Barlow M. J., 1975, MNRAS, 170, 41
Zimmermann L., Fuhrmann L., Massi M., 2015, A&A, 580, L2

This paper has been typeset from a TEX/LATEX file prepared by the author.